Fibers and Polymers
https://doi.org/10.1007/s12221-024-00523-6

Online ISSN 1875-0052
Print ISSN 1229-9197

REGULAR ARTICLE

An Evaluation of the Beneficial Effects of Polyamide 6's Thermal Stabilization by Ferric Chloride Complexation as a Novel Carbon Fiber Precursor

Tuba Demirel[1] · **Kemal Şahin Tunçel**[2] · **Ismail Karacan**[3]

Received: 26 September 2023 / Revised: 24 January 2024 / Accepted: 4 March 2024

Abstract
This study investigated the impact of stabilization time on pretreated polyamide 6 (PA6) fibers using various analytical techniques, including thermal analysis (TGA and DSC), infrared (IR) spectroscopy, X-ray diffraction (XRD), tensile testing, and density measurements. The two-step atmospheric air-based stabilization process for pretreated PA6 multifilament bundles involved initial thermal stabilization at 170 °C in an air atmosphere after ferric chloride impregnation, followed by a second step of thermal stabilization at 245 °C. Ferric chloride impregnation followed by thermal stabilization in an air atmosphere resulted in crucial structural transformations. The density values of the samples increased following thermal stabilization, accompanied by a decrease in tensile values. Ferric chloride pretreated and thermally stabilized PA6 fibers were found to be fully stabilized after 120 min of stabilization before the carbonization stage. The findings obtained from the DSC, XRD, and IR spectroscopy methods indicated the occurrence of disordering phases due to the scission of hydrogen bonds. The TGA findings showed significant increases in carbon yield percentages at 500 °C and 850 °C, reaching 71.4% and 63.5%, respectively, for the sample heat treated at 245 °C for 120 min. The addition of ferric chloride is expected to potentially reduce processing costs for final carbon fiber production by decreasing the time required for the thermal stabilization of PA6.

Keywords Polyamide 6 · Carbon fiber · Stabilization · Ferric chloride · Thermal analysis

1 Introduction

Carbon fibers (CFs) are widely acknowledged as one of the strongest and lightest materials used to reinforce advanced composite materials in construction [1]. The properties of CFs are influenced by various factors, including the structural composition of raw materials and the parameters used during production [2]. The production of CFs typically involves two stages: thermal stabilization and carbonization. During the stabilization stage, the thermoplastic precursor fibers are converted into a thermoset material [3, 4]. This process involves heating the fibers in ambient air within the temperature range of 200–300 °C for a specified period of time. The fibers absorb oxygen from the surrounding air, which is why this stage is also known as thermal oxidative stabilization (TOS). After stabilization, the fibers are annealed in an inert gas medium, usually nitrogen, at temperatures up to 2000 °C for a specific duration. During carbonization, the ratio of carbon atoms in the structure increases as non-carbon atoms are released in the form of volatile gases [5–7].

Polyamide 6, also known as Nylon 6, is an engineering thermoplastic with a range of versatile characteristics. It has a melting point (Tm) ranging from 210 to 220 °C, the ability to absorb moisture from the atmosphere typically within the range of 2.5–5%, and a density of 1.14 g/cm^3 [8–12]. Polyamides (PAs) are composed of a layer of planar zigzag conformation crystals, which create methylene sequences, and repetitive amide groups (–NH–C=O), giving rise to similar hydrogen bonding interactions [13].

Several research studies have investigated the production of CF from aliphatic linear chain polymer fibers as a new

✉ Kemal Şahin Tunçel
kemalsahintuncel@gmail.com

1 Department of Mechanical Engineering, Hasan Kalyoncu University, 27410 Gaziantep, Turkey

2 Department of Traditional Crafts, Siirt University, 56100 Siirt, Turkey

3 Department of Nano Science and Nano Technology, Erciyes University, 38039 Kayseri, Turkey

Published online: 19 March 2024

precursor [14–18]. The presence of amide and carboxylic and amino end groups influences the stabilization of polyamides. If chemical pretreatment is not used during the stabilization of polyamides, the procedure becomes time-consuming [14]. To improve the stabilization of PA6, a metal salt such as Cu, Cd, Mn, Ca, Zn, alkali metals, or Fe can be used as a potent antioxidant inhibitor [19]. Chemical impregnation of precursor fibers with complexes formed between polymers and metals accelerates thermochemical reactions and simplifies the development of a cross-linked polymer structure [17]. This study proposes the use of textile-grade polyamide 6 fibers as a cost-effective alternative precursor for low-cost carbon fiber production due to its relatively high carbon content, widespread availability in global markets, lower cost, recyclability, and ease of processing. According to published data, polyamide 6/66 fibers account for 6 million metric tons of production per year by 2022. The aim of this research is to examine the effect of impregnating PA6 fibers with $FeCl_3$ salt before subjecting to TOS. The interaction between the $FeCl_3$ metal halide and PA6 fibers has been extensively studied. Therefore, this study is expected to provide valuable insights to other experimental studies in this field. Various characterization techniques, including TGA, DSC, IR spectroscopy, XRD, tensile testing, and density measurements, were employed to assess the results obtained in the course of the experimental study.

2 Materials and Methods

The PA6 multifilament bundle examined in this study has a yarn count of 15.8 tex and is composed of 48 filaments. The PA6 polymer composition includes 66.06% carbon (C), 12.84% nitrogen (N), 10.09% hydrogen (H), and 11.01% oxygen (O). The measured fiber diameter is 19.9 µm. Anhydrous ferric chloride (99% purity) was obtained from Kimetsan AS (Turkey), and a 1% (w/w) aqueous solution of $FeCl_3$ was used to impregnate untreated PA6 fibers before the TOS stage. The linear density of the PA6 fibers impregnated with a 1% (w/w) $FeCl_3$ aqueous solution is 17.6 ± 0.59 tex, with an impregnation ratio of 11.4%. The pH of the solution was found to be 1.93 at room temperature. Figure 1 illustrates the complexation mechanism between PA6 polymer chains in the presence of $FeCl_3$ as a cross-linking agent. Initially, untreated PA6 exhibits intermolecular hydrogen bonding among amide groups. However, after chemical pretreatment and thermal stabilization, a decreasing trend in hydrogen bond formation is observed. Following impregnation, the fibers undergo thermal stabilization through a two-step annealing process, as shown in Fig. 2.

Density measurements were conducted using mixtures of isopropyl alcohol ($\rho = 0.79$ gr/cm^3) and perchloroethylene ($\rho = 1.612$ g/cm^3) and the average of five measurements was

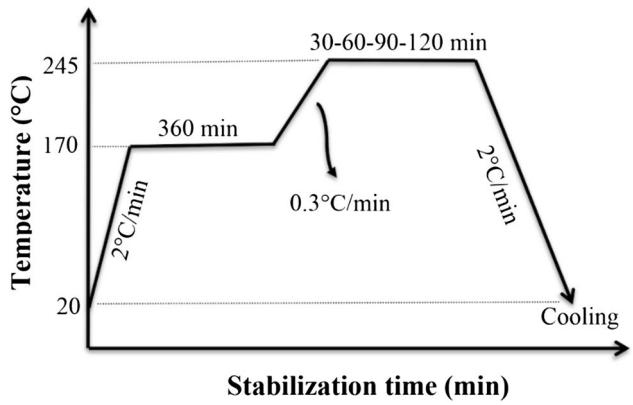

Fig. 2 Two-step annealing procedure for PA6 fibers impregnated in 1% $FeCl_3$ solution

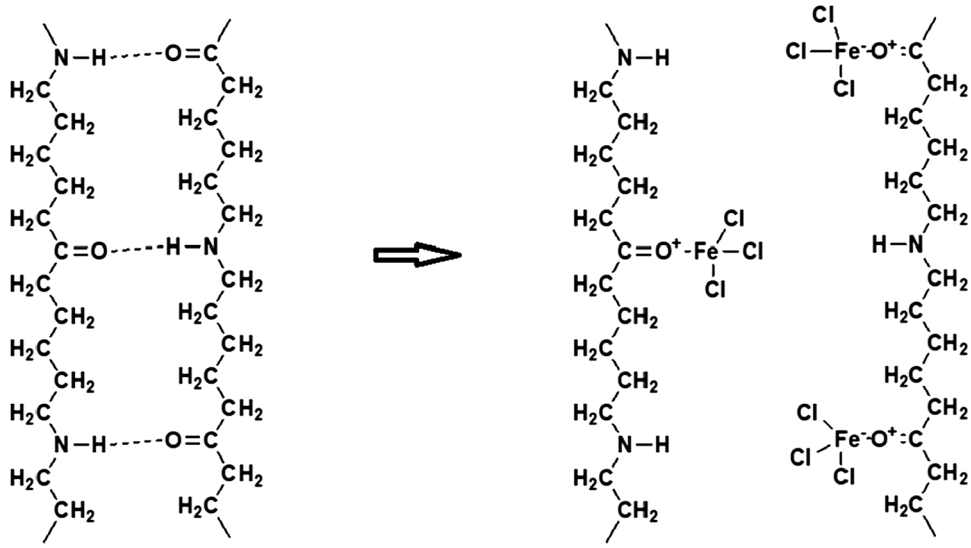

Fig. 1 The mechanism of forming a complex between polyamide 6 and $FeCl_3$

taken. Mechanical properties were assessed using a Prowhite tensile machine at a constant drawing rate of 5 mm/min and a gauge length of 20 mm, with reported findings representing the average of ten tensile tests. Thermal analysis graphs were generated using a Perkin Elmer TGA diamond system, where specimens were heated at a rate of 10 °C/min up to a maximum temperature of 850 °C in a continuous flow of nitrogen gas. IR measurements were conducted using a PerkinElmer Spectrum 400 spectrometer with a scan range from 3750 to 900 cm^{-1} and a wavenumber resolution of 2 cm^{-1}. The diffraction measurements were conducted using the Bruker AXS D8 X-ray diffractometer, with voltage and current settings of 40 kV and 40 mA, respectively, covering the 2θ angle range from 5° to 40°. DSC experiments were performed using a PerkinElmer Diamond DSC system, heating samples at 10 °C/min up to a maximum temperature of 340 °C, and the sample weight was about 5 mg.

3 Results and Discussion

3.1 Fiber Density

Thermal stabilization is an essential stage in the production of carbon fibers, typically carried out in ambient air. The duration of this process significantly influences the chemical composition of PA6 fibers. Figure 3 illustrates the density measurements of untreated and stabilized PA6 fibers over time, spanning from 0 to 120 min. The density values consistently raised as the annealing process progressed, reaching 1.35 g/cm^3 during the final stabilization period, which is the 120-min mark. Similar to the stabilization of polyacrylonitrile fibers, an increase in fiber density values is observed with prolonged annealing durations [20].

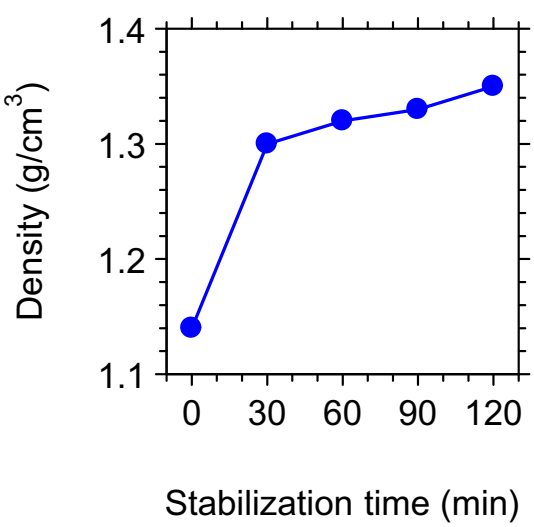

Fig. 3 Volume density values of untreated and stabilized PA6 samples depending on stabilization time

The increase in density values observed in PA6 fibers following the stabilization process primarily arises from the elimination of non-carbon constituents and the subsequent reconfiguration of the polymer's chemical composition [21]. PA6 fibers contain not only carbon, but also other elements such as hydrogen, oxygen, and nitrogen within their molecular structure. During the stabilization stage, which requires subjecting the fibers to elevated temperatures within an oxygen-rich environment, these non-carbon constituents undergo gradual removal in the form of volatile gases. This removal leads to a reduction in the overall mass of the fiber, while the carbon content remains preserved.

Simultaneously, as the non-carbon elements are expelled, the carbon atoms in the polymer chains undergo rearrangement, often leading to the formation of cross-links and the creation of aromatic ring structures within the polymer. These changes result in a more tightly packed and ordered carbon structure [21]. The removal of non-carbon atoms and the development of a more ordered carbon structure lead to a reduction in the free volume within the polymer. This means that the carbon atoms are packed closer together, increasing the fiber's density [22]. Typically, higher temperatures and prolonged stabilization yield more substantial density increments. However, careful control of these conditions is imperative to avoid undesired consequences such as fiber degradation.

3.2 Tensile Properties

Changes in mechanical properties such as tensile strength, tensile modulus, and extension at the break of untreated and stabilized samples are presented in Fig. 4. Additionally, stress–strain curves for each sample are shared in Fig. 5. The tensile strength and modulus values exhibit a declining trend as the duration of stabilization increases, as illustrated in Fig. 4. Untreated PA6 fibers display the highest tensile strength, measuring 217 MPa, whereas PA6 fibers subjected to 30 min of stabilization show a tensile strength of 83 MPa (Fig. 4a). Additionally, the tensile modulus of PA6 fibers stabilized for 30 min is measured at 12.5 GPa. The existence of Fe^{+3} likely disrupts hydrogen bonds between the molecular chains of PA6. This is because ferric ions primarily form complexation bonds with the carbonyl (C=O) groups, leaving N–H bonds free without hydrogen bonding (as shown in Fig. 1). The disruption of hydrogen bonding is a central factor contributing to the observed decrease in tensile strength with the incorporation of ferric chloride, particularly in relation to the duration of the stabilization process.

The tensile modulus experiences a rapid decline, reaching approximately 12.5 GPa immediately after a 30-min two-step annealing process for the sample treated with a 1%

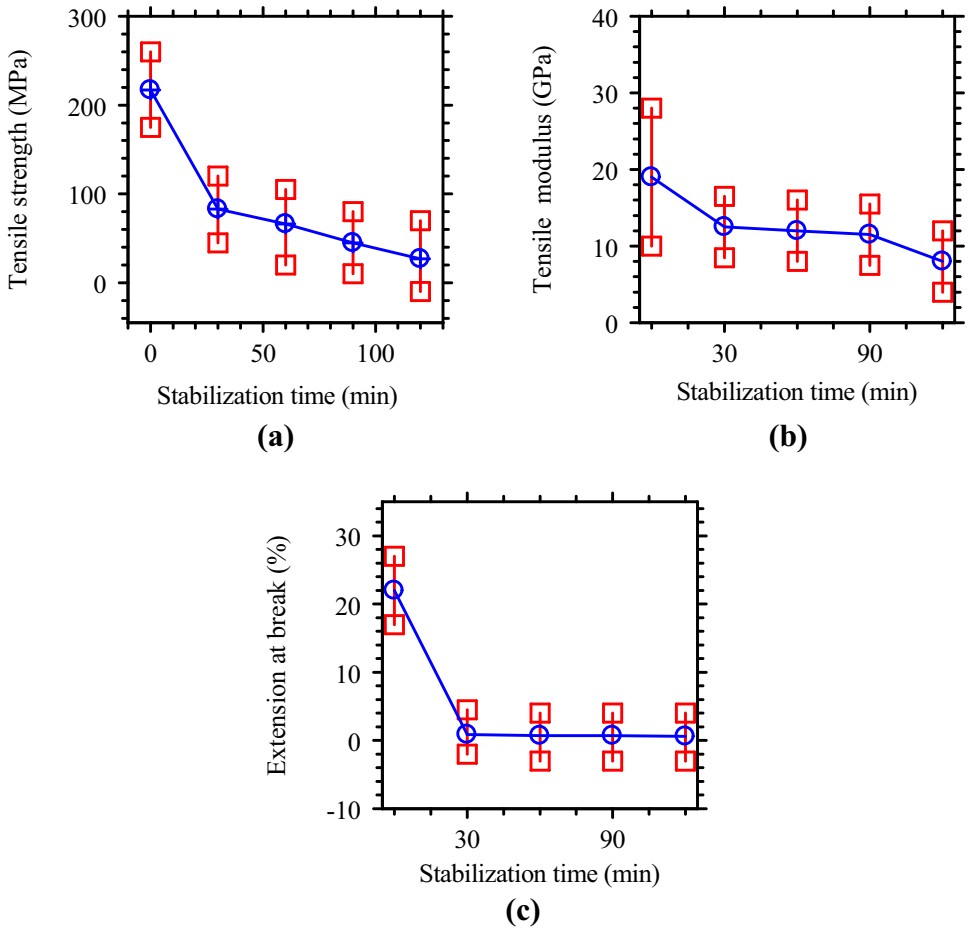

Fig. 4 Variation of **a** tensile strength, **b** tensile modulus, **c** extension at break (%) values of untreated and stabilized PA6 samples depending on stabilization time

$FeCl_3$ aqueous solution. 1% $FeCl_3$ aqueous solution-impregnated and stabilized PA6 fibers' tensile modulus was found to be 8 GPa for a stabilization time of 120 min (Fig. 4b). This observation highlights a reduction in tensile modulus values, with a notable initial decrease at the 30-min stabilization, followed by a continuous and consistent decline over time. Extension at break values presented in Fig. 4c shows decreasing values with rising stabilization time. The decline in this value resulted in the transformation of the PA6 samples into a fragile structure. The tendency for a decline in the mechanical properties of PA6 fibers following thermal stabilization is a phenomenon that can similarly be observed when producing carbon fibers from PAN-based fibers [1, 21, 23].

The decrease in mechanical properties such as tensile strength and modulus following the stabilization of PA6 samples in carbon fiber production may be due to many reasons. High-temperature exposure during the stabilization stage can lead to the loss of molecular mobility and result in the fusion of polymer chains. As a consequence, the fiber becomes more rigid and less ductile [24], which can cause a reduction in tensile properties (as shown in Fig. 4c). Hydrogen bonds play a crucial role in enhancing the strength and flexibility of fibers. However, the mechanical properties are adversely impacted by the disruption of these bonds resulting from chemical pretreatment and the subsequent stabilization process.

It is important to note that while the initial stabilization process may lead to a decrease in certain tensile properties, it is a necessary stage in the production of carbon fibers. Subsequent processing stages, including carbonization, further transform the fiber to enhance its tensile properties, resulting in high-strength carbon fibers.

3.3 X-ray Diffraction (XRD)

As per findings reported in the existing literature [25], XRD assessments have revealed the coexistence of both α- and γ-crystalline forms within the stretched PA6 multifilament bundle. Both of these crystal structures exhibit monoclinic configurations, each featuring distinct arrangements of hydrogen bonding networks among polymer chains. Moreover, both crystal forms exhibit monoclinic unit cells, with the b-axis oriented as the primary axis parallel to the fiber direction [26–28]. It has been proposed that the reconfiguration of hydrogen bonds leads to the formation of distinct

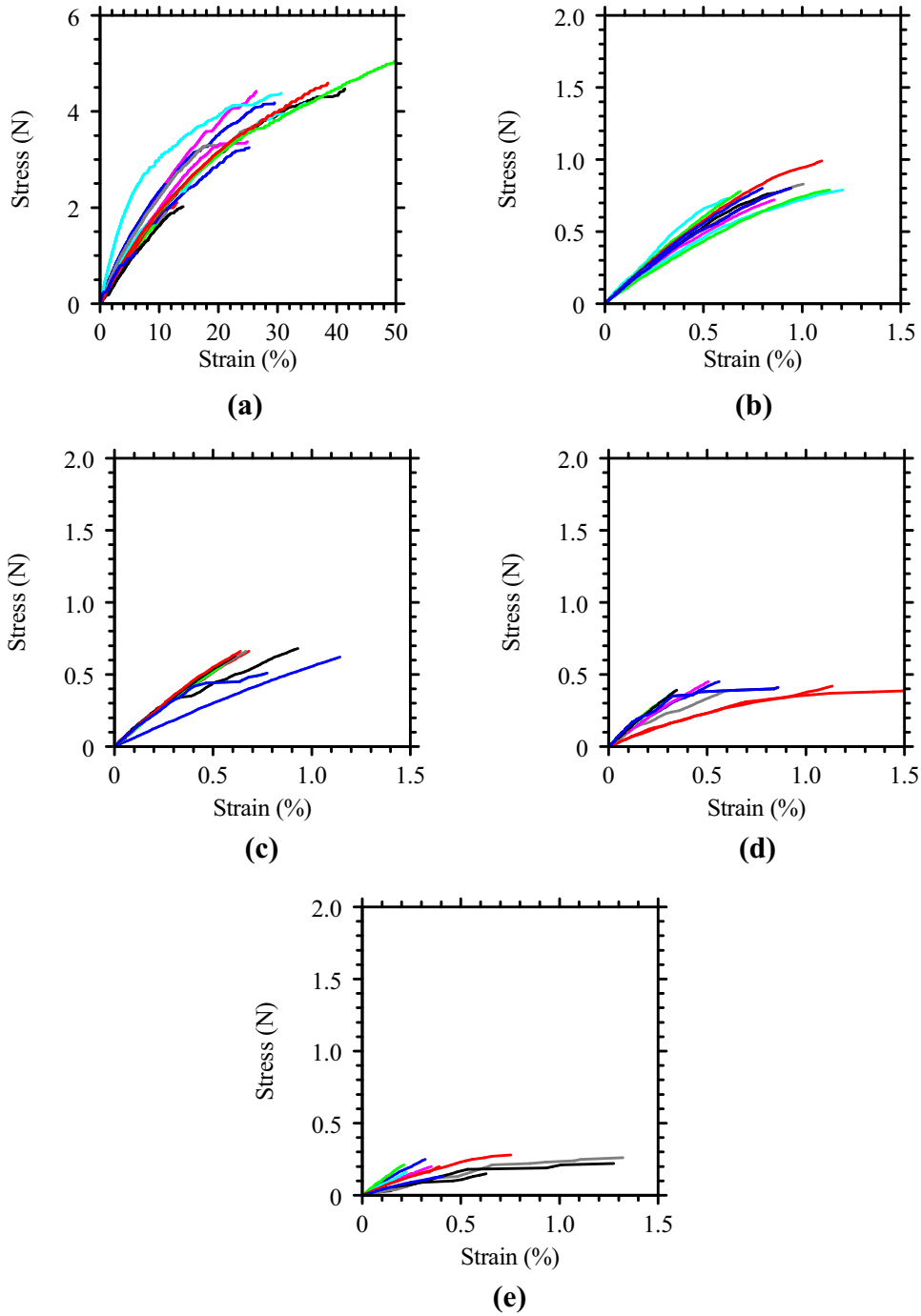

Fig. 5 Stress–strain curves of original and 1% FeCl3 aqueous solution-impregnated stabilized PA 6 fibers as a function of stabilization conditions: **a** untreated PA6 **b** 245 °C at 0.3 °C/min, 30 min **c** 245 °C at 0.3 °C/min, 60 min **d** 245 °C at 0.3 °C/min, 90 min **e** 245 °C at 0.3 °C/min, 120 min

crystal structures. Specifically, it is anticipated that the distance between the amide groups would be greater in the α-crystalline form compared to the γ-crystalline form. This variation in hydrogen bonding behavior within the γ-crystalline structure is expected to result in reduced interactions between polymer chains compared to the α-phase. According to existing literature, the α-form crystalline phase is typically found at room temperature. Interestingly, it has been observed that the α-form crystalline structure can undergo a transformation into the γ-crystalline phase through processes such as iodination, followed by iodine extraction using substances like water, acetone, ethylenediamide [29], or sodium thiosulfate [30]. Additionally, high-speed melt spinning of the PA6 multifilament bundle appears to induce the formation of the γ-phase structure [30, 31]. Furthermore, electrospun PA6 nanofibers have demonstrated the presence of the γ-crystalline form, which can subsequently convert to the more stable α-form crystalline structure through heat treatment at temperatures exceeding 150 °C [32]. It seems that the crystal structures of α- and

γ-forms exhibit different density values. As a result of the formation of different crystalline structures, the observed density value of α-form is 1.23 g/cm^3, whereas the observed density value of γ-form is 1.17 g/cm^3 [33].

Figure 6 illustrates equatorial XRD patterns for both untreated and stabilized PA6 samples over varying stabilization times. In addition to the crystalline peaks, an additional set of four reflections was identified with peak positions at 11, 24.8, 25.7, and 35º (2θ) [34]. These reflections (correspond to the $FeCl_2{\cdot}4H_2O$ crystal structure) have been identified and indexed as (100), (020), (210), and (320) reflections originating from a monoclinic unit cell with specific dimensions: *a*: 1.175 nm, *b*: 0.709 nm, *c*: 0.849 nm, and *β*: 111.15º (2θ) [30].

It seems that a portion of $FeCl_3{\cdot}6H_2O$ undergoes a reduction to $FeCl_2{\cdot}4H_2O$ during impregnation and thermal stabilization processes. The XRD traces associated with ferric chloride indicate that the chemical impregnation process extends to both the amorphous and crystalline phases of PA6 samples, respectively. The peak separation in the equatorial XRD pattern of the untreated PA6 sample, as depicted in Fig. 7, indicates the presence and simultaneous coexistence of a polymorphic structure comprising both α- and γ-crystalline forms alongside an amorphous phase.

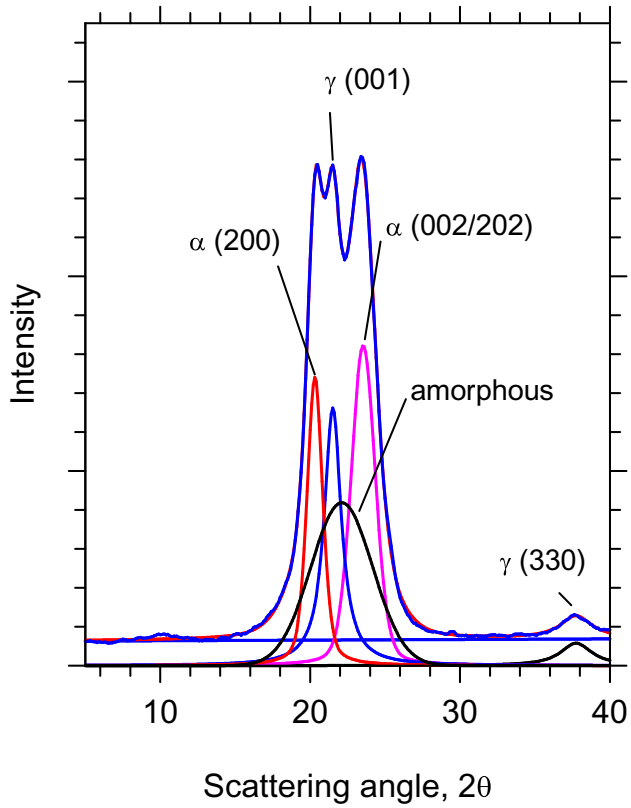

Fig. 7 Peak separation of XRD profile of untreated PA6 multifilament bundle

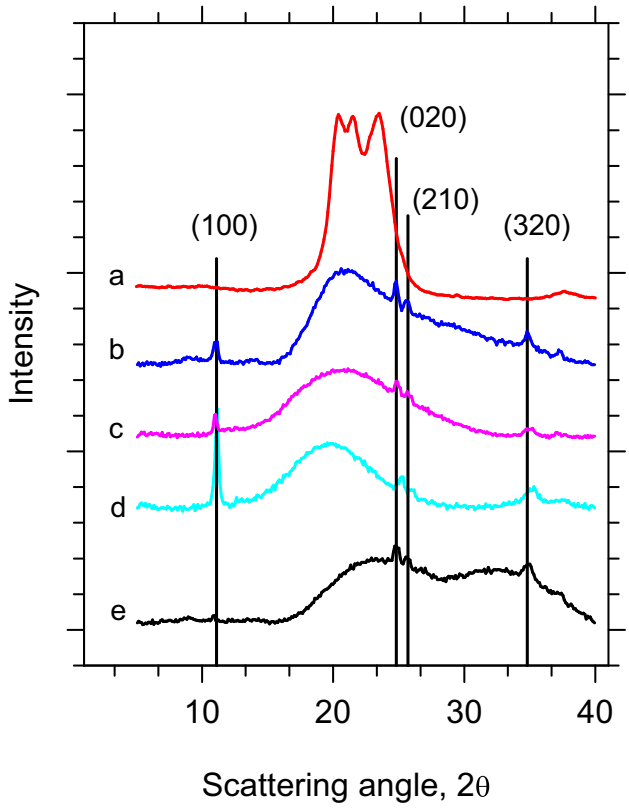

Fig. 6 XRD traces of untreated and stabilized PA6 multifilament depending on stabilization time. (a) Untreated PA6, (b) 30 min, (c) 60 min, (d) 90 min, (e) 120 min

3.4 Infrared Spectroscopy (FT-IR)

An in-depth analysis of structural alterations occurring during the thermal stabilization process was carried out using IR vibrational spectroscopy. The emergence of unbound N–H peaks is attributed to the occurrence of complexation reactions between ferric ions and the oxygen in the carbonyl (C=O) group of the amide unit. The bonding of Fe^{+3} cations with carbonyl oxygen results in the disruption of hydrogen bonds within the structure, leading to the liberation of N–H bonds. Specifically, the peaks located at 3270 cm^{-1} (N–H stretching) and 1630 cm^{-1} (C=O stretching), vibrations, participate in hydrogen bonding interactions at precursor fiber structure [35]. Especially noteworthy is that alterations in phase fractions do not impact the peak position of the N–H band involved in hydrogen bonding. The variations in intensity and spectroscopic alterations were investigated in relation to the duration of the stabilization process.

Figure 8A showcases the IR spectra within the 3750–2450 cm^{-1} range for untreated PA6, $FeCl_3$-impregnated followed stabilized samples. The infrared

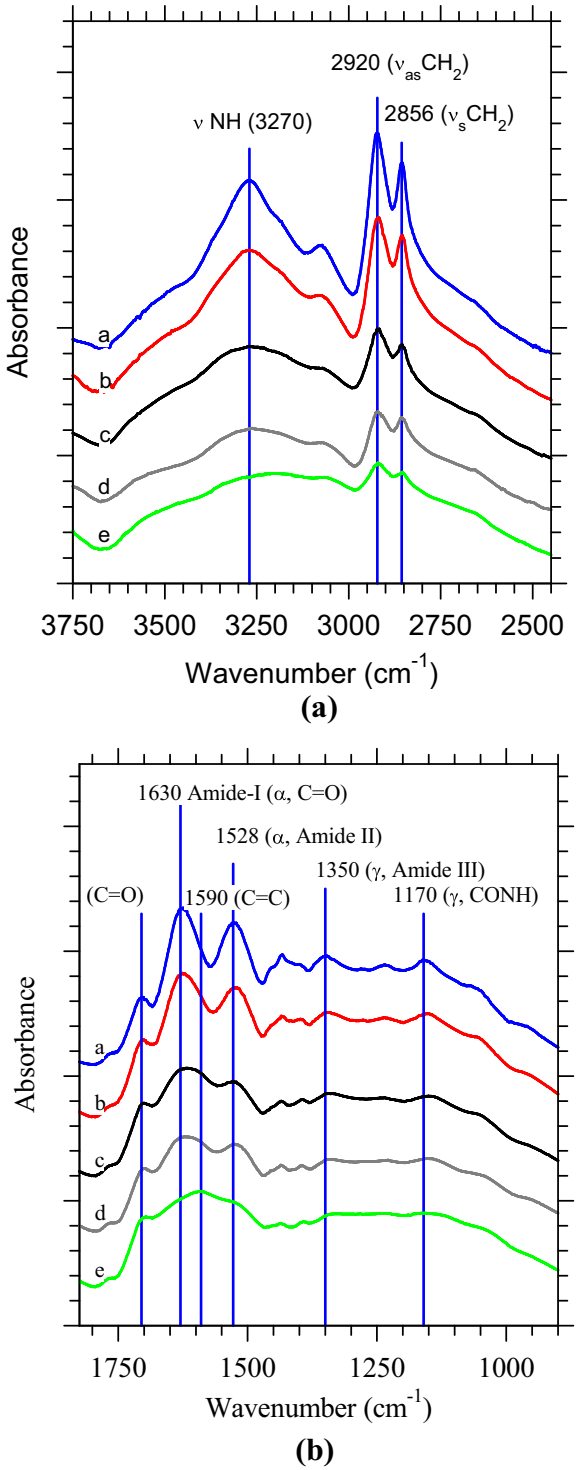

Fig. 8 FT-IR spectra at **A** 3750–2450 cm^{-1}, **B** 1825–900 cm^{-1} of the experimental PA6 samples, (a) untreated PA6, (b) 30 min, (c) 60 min, (d) 90 min, (e) 120 min

(IR) spectral region ranging from 3500 to 3100 cm^{-1} is attributed to the stretching vibrations of hydrogen-bonded N–H groups. In pristine PA6, these intermolecular hydrogen bridges occur between NH–C=O groups of adjacent polymer chains. As illustrated in Fig. 8A, untreated PA6 fiber displays a nearly 100% prevalence of hydrogen-bonded chains [36], indicated by the absence of peaks above 3300 cm^{-1}. The alterations observed in the N–H band following treatment with metal halides lead to modifications in the conformation of PA6 chains, transitioning them from a "trans" to a "cis" configuration [36]. It is quite likely that the changes observed, including the loss of hydrogen bonds due to the complexation between the amide groups and ferric ions, could also lead to similar transformations. The amide I vibration, observed at 1630 cm^{-1} (Fig. 8B), is predominantly associated with the stretching vibrations of the carbonyl (C=O) groups. In this study, it has been observed that the initial structure of pristine PA6 chains is primarily in the trans-conformation, as evident from the vibration at the wavenumber of 3270. The location of N–H vibration involved in hydrogen bonding was documented to shift toward higher wavenumbers [37]. Furthermore, the introduction of gallium-trichloride ($GaCl_3$) as a Lewis acid into the PA6 structure led to a significant forward at the position of the N–H vibration [38]. After the impregnation of ferric chloride and following the two-step annealing approach, the infrared spectra displayed substantial alterations in intensity, particularly in relation to the peaks NH and CH_2 stretching vibration.

The IR traces of heat-treated samples showed the appearance of a wide-ranging free N–H band covering the region between 3600 and 3350 cm^{-1}. Besides, numerous peaks associated with amide I, amide II, and amide III vibrations were observed, alongside various crystalline and amorphous vibrations. Interestingly, the location of methylene vibrations remained unaffected by the introduction of $FeCl_3$ into the PA6 structure. This outcome was unexpected but the C–H bands within the 3000–2800 cm^{-1} range are generally not influenced by complexation, as these vibrations do not play a significant role in hydrogen bond formation [39]. Furthermore, the IR band at 3270 cm^{-1}, attributed to hydrogen-bonded NH vibrations, exhibited a gradual decrease in intensity with increasing stabilization time, signifying the dissociation of hydrogen bonds (Fig. 9a). Notably, in the sample heat treated at 245 °C for 120 min, the intensity of the hydrogen-bonded N–H vibration at 3270 cm^{-1} nearly vanished completely, indicating the complete disruption of hydrogen bonds between the amide groups of polymer chains. This observation further corroborates the extensive involvement of hydrogen-bonded N–H groups in complexation with ferric ions.

The methylene (CH_2) vibrations at 2920 and 2856 cm^{-1} experienced a significant reduction in intensity as the stabilization time increased, yet some residual intensity remained, suggesting that not all hydrogen species were involved in the dehydrogenation reactions (Fig. 9b). The

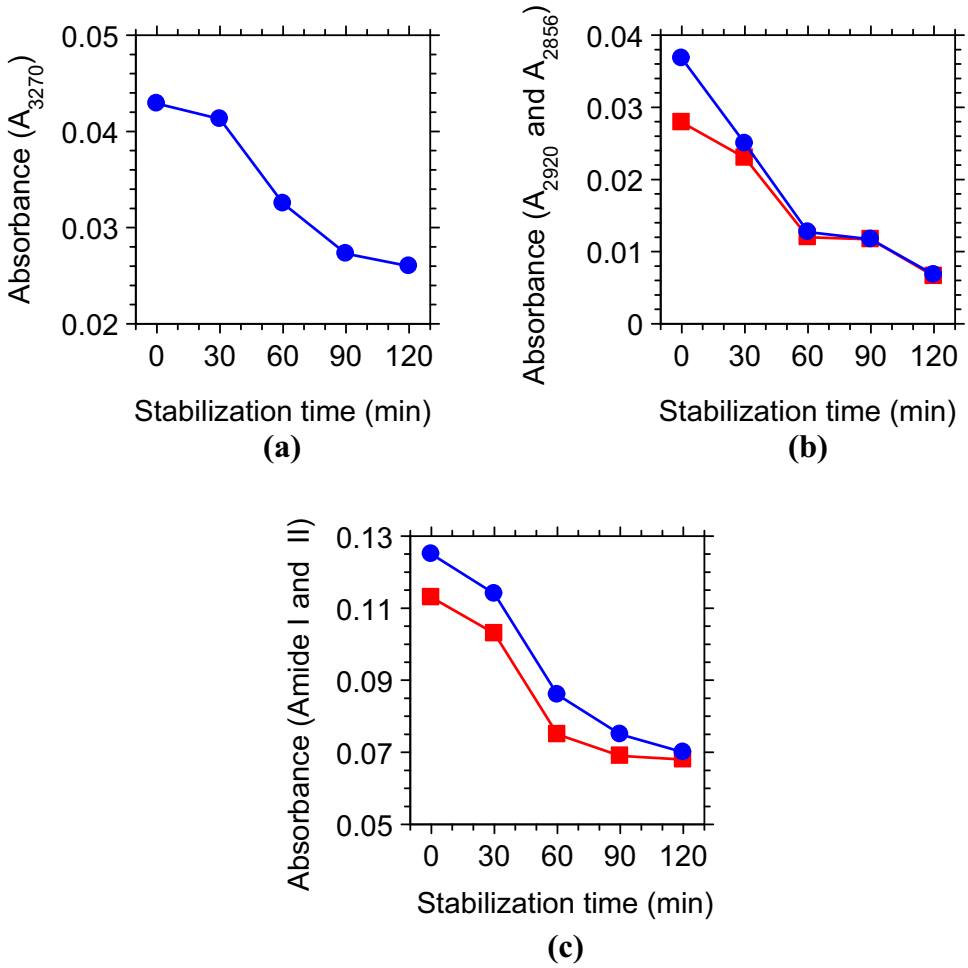

Fig. 9 Examining the change in absorbance value depending on the stabilization time of certain IR vibrations: **a** 3270 cm^{-1}; **b** 2856 and 2920 cm^{-1} (□ 2856 cm^{-1}, ◯ 2920 cm^{-1}); **c** amide I and II peaks (◯, amide I; □, amide II)

decline in the trace of the methylene vibrations serves as a distinct indicator that dehydrogenation indeed appeared during two-step annealing processes. As stabilization time increased, the traces of NH and methylene groups, located at 3270, 2920, and 2856 cm^{-1}, showed a gradual reduction but did not completely vanish. Moreover, the half-widths of the hydrogen-bonded N–H and methylene bands were observed to widen with an increasing stabilization period.

The IR spectra of the two-step annealing samples showed the emergence of a newly discovered peak position at 1705 cm^{-1}, ascribed to carbonyl vibration, which resulted from thermal stabilization reactions, and this band's traces steadily increased with extended annealing time. In Fig. 8B, the most prominent bands were amide I and amide II peaks at 1630 and 1528 cm^{-1}, respectively. Meanwhile, the infrared peaks associated with the α-phase, positioned at 1316, 1200, and 930 cm^{-1}, experienced a significant reduction in intensity as stabilization time increased. Similarly, infrared peaks associated with the γ-phase, located at 1236 and 973 cm^{-1}, also exhibited a notable decrease in intensity with prolonged stabilization time, likely due to the initiation of an amorphization event, potentially caused by the disruption of hydrogen bridges among the polymer chains.

In the IR spectra of samples subjected to stabilization times ranging from 30 to 120 min, noteworthy frequency shifts were observed. The amide I peak, initially at a wavenumber of 1630, progressed to a lower peak position at a wavenumber of 1625, which suggests the connection of Fe^{+3} ions with the C=O vibration. Similarly, the amide II peak at a wavenumber of 1528 progressed to a lower peak position at a wavenumber of 1522. The amide II peak arises primarily from N–H in-plane bending and is expected to change peak position when Fe^{+3} ions form a connection with the carbonyl oxygen. This action leads to the breakage of hydrogen bridges, thus freeing the N–H groups. In the sample stabilized for 120 min, broadband appeared at 1590 cm^{-1}, indicating the presence of C=C bonds, signifying the formation of intramolecularly cross-linked structures.

Figure 9c illustrates the changes in the intensity of amide I and II vibrations relative to the stabilization duration. It is evident that the intensities progressively diminish with extended time due to the take place of an amorphization event. The altered positions of the amide I and II peaks

remained relatively stable during the initial phases of stabilization. However, as the stabilization period reached 120 min, most of the band intensities diminished significantly due to the initiation of decrystallization and dehydrogenation reactions triggered by the introduction of ferric ions into the PA6 structure.

3.5 Thermogravimetric Analysis (TGA)

Thermal analysis of untreated PA6 fibers, as well as those impregnated with $FeCl_3$ and subsequently stabilized, was conducted through TGA. The weight losses occurring within a narrower temperature range correspond to faster decomposition processes, leading to more pronounced weight reductions and consequently lower carbon yields. For untreated PA6, thermal stability is maintained up to 300 °C, followed by a significant weight loss. Afterward, a more rapid and substantial decomposition process occurs, extending up to 485 °C (see Fig. 10A).

The PA6 sample in its original state experiences a weight loss of approximately 98% at 850 °C, leaving a carbon yield of 2.2%. Upon treatment with ferric chloride and subsequent annealing, the TGA charts of PA6 samples indicate that the initial stage involves the removal of surface-bound water vapor up to about 100 °C. Subsequently, there is a significant rise in the weight loss rate between 300 and 500 °C, which can be attributed to the catalytic influence of Fe^{+3} ions. These ions are actively involved in the decomposition events of the PA6 material [40]. Figure 10B presents the TGA charts of $FeCl_3$-impregnated and heat-treated PA6 materials, demonstrating a reduction in weight loss with extended annealing duration, indicative of an increased carbon yield. This increase can be attributed to the growing intermolecular cross-linking reactions occurring between the PA6 polymer chains. The original PA6 material experiences weight loss within a limited temperature span, while annealing materials exhibit weight loss across a broader temperature span. This phenomenon is attributed to the enhanced formation of ladder-like structures through intensified intermolecular cross-linking.

Figure 10B presents the carbon yield values of all experimental samples at 500 and 850 °C. The experimental investigations conducted on ferric chloride-impregnated and stabilized PA6 samples demonstrated highly efficient aromatization and dehydrogenation reactions. The development of unsaturated sites as a result of hydrogen loss during dehydrogenation processes facilitated the occurrence of intermolecular cross-links, leading to a substantial increase in carbon yield.

Ferric chloride played a crucial role in facilitating coordination bonds between the carbonyl oxygen of amide (–NH–C=O) groups. This promoted the formation of intra and intermolecular processes that resulted in the development of highly aromatic and cross-linked structures. The analysis of TGA charts suggests that intensified interactions between ferric ions and the amide bonds within PA6 sample reactions led to the generation of both intramolecular and intermolecular cross-linking reactions. This ultimately resulted in the production of significant amounts of carbonized entities in a nitrogen atmosphere.

Figure 10B shows that carbon yield values increase continuously with increasing stabilization time. At 500 °C, carbon yields range from 2.7 to 71.4%, surpassing those at 850 °C. The $FeCl_3$-impregnated PA6 samples that underwent

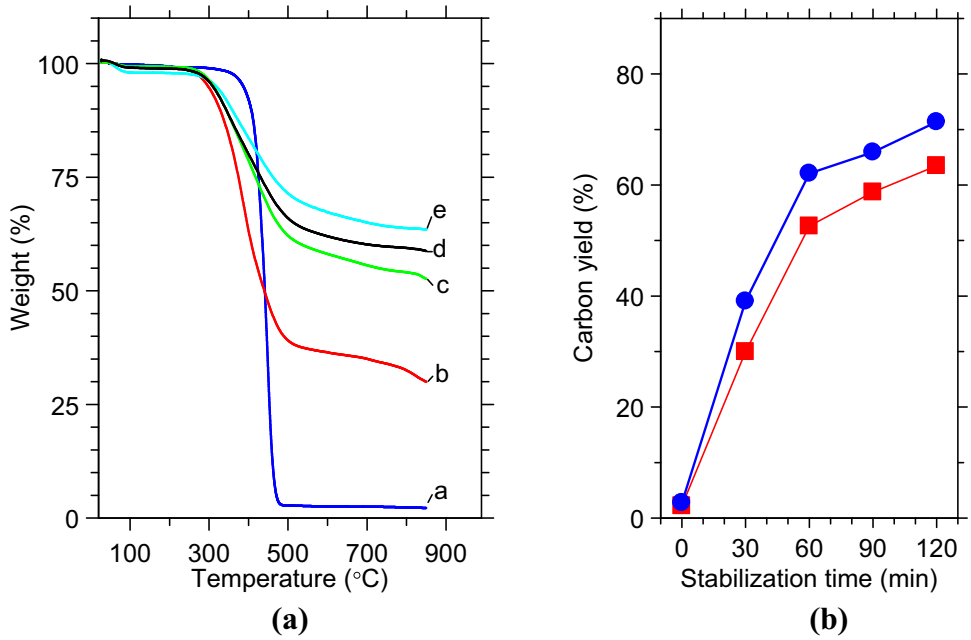

Fig. 10 **A** TGA thermograms of experimental samples depending on stabilization time. (a) Untreated PA6, (b) 30 min, (c) 60 min, (d) 90 min, (e) 120 min. **B** Comparison of carbon yield values of untreated and stabilized PA6 samples at different temperatures (empty circle) 500 °C; (□) 850 °C

a 120-min stabilization period achieved the highest carbon yield of 63.5% at 850 °C. The TGA charts show that adding ferric chloride and thermally stabilizing the PA6 samples improves their thermal stability compared to the original PA6 sample. This is mainly due to cross-linking reactions.

3.6 Differential Scanning Calorimetry (DSC)

The DSC thermograms of both pristine and 1% $FeCl_3$-impregnated PA6 fibers are illustrated in Fig. 11A. In the DSC thermogram of untreated PA6 fibers, a prominent melting endotherm is observed, situated around 222 °C [41]. Across all DSC thermograms, a minor endotherm in the 40–110 °C range is noticeable, attributed to the presence of surface moisture on the samples. As depicted in Fig. 11A, the incorporation of 1% $FeCl_3$ into PA6 fibers leads to a slight reduction in the melting point, down to 219 °C. This observation suggests that the introduction of ferric ions (Fe^{+3}) results in a decrease in the melting temperature. Previous studies have reported a decrease in melting point and crystallinity when incorporating metal halide salts, such as $FeCl_3$, $CuCl_2$, and $CuBr_2$, into the PA6 polymer. Furthermore, it is important to note that copper halides exhibit a more significant decrease in melting point compared to iron halides [42].

According to the literature, the glass transition temperature (Tg) of PA6 increases as the content of cupric ions (Cu^{+2}) from cupric chloride ($CuCl_2$) increases. However, it is important to note that the rate of Tg increase was reported to be more significant for the ferric chloride ($FeCl_3$) system compared to the cupric chloride ($CuCl_2$) system when both systems had similar metal halide content [43]. Figure 11B displays the DSC thermograms of PA6 samples that underwent thermal stabilization with varying times, namely 30, 60, 90, and 120 min. Notably, the melting points of samples stabilized for 30 and 60 min increased to 225 and 227 °C, respectively. This suggests that cyclization reactions commenced during the early stages of the thermal stabilization process due to ongoing cyclization and aromatization reactions as the stabilization time increased. In the DSC thermograms depicted in Fig. 11B, the complete absence of melting endotherms with the prolongation of the two-step annealing process indicates the outcome of the cyclization and aromatization reactions.

During the examination, decomposition peaks were observed at 300ºC. These peaks exhibited a decrease in intensity as the stabilization time progressed, suggesting that temperature stability is achieved after a 120-min stabilization process at 245 °C. The coordination of Fe^{+3} ions with the carbonyl oxygen (C=O) of the amide (NH–C=O) groups facilitates the cyclization and aromatization reactions of PA6 molecular chains. This results in the formation of ring-like structures that contain at least five or six carbon atoms, which exhibit high resistance to elevated temperatures. It is highly likely that Fe^{+3} ions coordinate with the carbonyl oxygen (C=O) of the amide (NH–C=O) groups. As ferric ions (Fe^{+3}) form complexation bonds with the carbonyl (C=O) groups, the N–H groups are left unbound by hydrogen, thus leading to the disruption of hydrogen bonding. This disruption of hydrogen bonding is one of the primary factors contributing to the reduction in melting points following the incorporation of ferric chloride.

The complexation between ferric ions and the amide (N–H–C=O) groups is anticipated to primarily occur within the highly disordered regions due to the relatively easy access of ferric ions into such regions. As the thermal

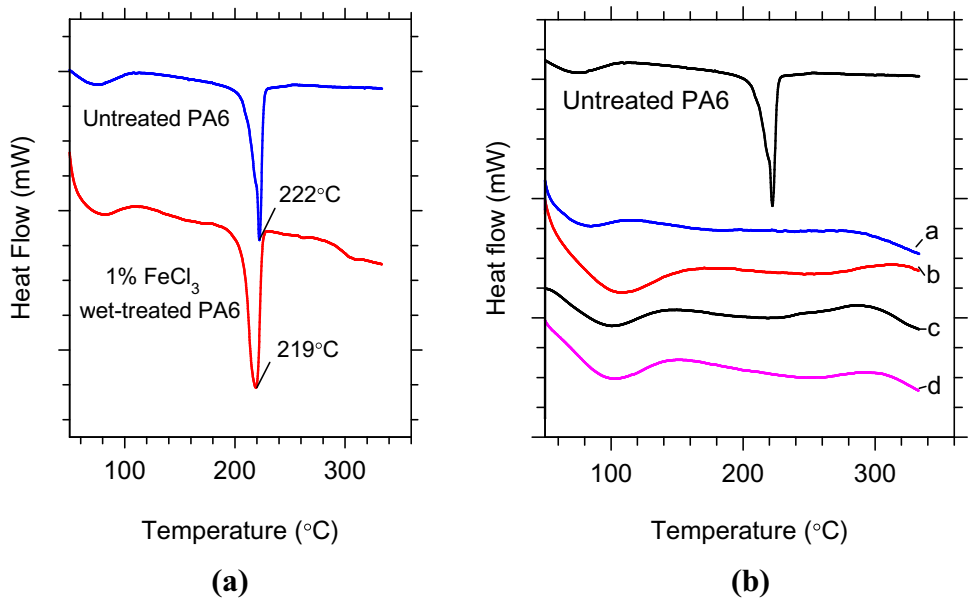

Fig. 11 **A** DSC thermograms of untreated PA6 and 1% $FeCl_3$ wet treatment sample. **B** DSC thermograms of stabilized PA6 samples depending on the stabilization period. (a) 30 min, (b) 60 min, (c) 90 min, (d) 120 min

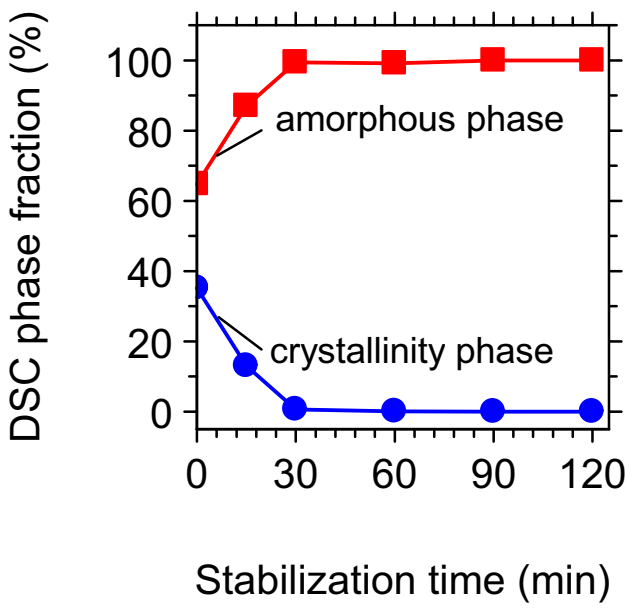

Fig. 12 DSC-crystallinity (◯) and amorphous fraction (□) of untreated and stabilized PA6 fibers depending on the stabilization period

stabilization process progresses, this interaction is likely to extend into the ordered, crystalline regions by disrupting the hydrogen bonding network. This process is further enhanced and facilitated by the contribution of heat energy [44]. With increasing stabilization time at 245 °C, it becomes evident that the melting enthalpy (ΔH) decreases due to ongoing amorphization processes. The melting enthalpy values are commonly used to assess the degree of crystallinity, and it's worth noting that the maximum ΔH value for 100% PA6 polymer is 190 J/g [45]. The structure of oriented PA6 fiber typically features a polymorphic crystal form comprising a combination of the more stable α-phase and the less stable γ-phase [25]. The γ-crystal form is known to remain stable up to 170ºC, transitioning to the more stable α-phase at higher temperatures [46]. Therefore, the melting enthalpy values evaluated above 170ºC in the DSC thermograms are associated with the α-phase. The DSC crystallinity values decrease progressively with increasing stabilization time due to ongoing decrystallization reactions. For instance, the DSC crystallinity value decreases from 35.2% for the untreated sample to 0.1% for the sample stabilized for 60 min. The results plotted in Fig. 12 illustrate a decreasing trend in DSC crystallinity and a corresponding increasing trend in the amorphous fraction depending on the stabilization period. DSC crystallinity decreases from 35.2 to 0%, while the amorphous fraction increases from 64.8 to 100%. These changes in melting point and the formation of amorphous structures are directly attributed to the strong interaction between Fe^{+3} and the amide segments within the PA6 molecular chains.

4 Conclusions

The influence of stabilization time on pretreated PA6 fibers was investigated using various analytical techniques, including thermal analysis (TGA and DSC), infrared spectroscopy, X-ray diffraction, tensile testing, and density measurements. The use of a partially oriented PA6 precursor, along with 1% FeCl3 impregnation for stabilization, demonstrated the potential to reduce both stabilization time and temperature. This phenomenon was accomplished by creating a molecular structure that is highly stabilized. The study utilized a two-step atmospheric air-based stabilization process for pretreated PA6 multifilament bundles. The first stage involved thermal stabilization at 170 °C in an air atmosphere following ferric chloride pretreatment. Subsequently, the second stage entailed thermal stabilization at 245 °C. Pretreatment of PA6 fibers with a 1% $FeCl_3$ aqueous solution was found to enhance the thermal stability and density of samples. The experimental findings suggest that pretreatment in the 1% $FeCl_3$ aqueous solution optimized the stabilization time and facilitated the rapid development of the cyclization structure. As the stabilization time increased, the IR results revealed accelerated aromatization and dehydrogenation reactions. This supported the formation of (C=C) bonds and aromatic structures. IR spectroscopic and XRD results indicated a gradual decrease in crystallinity due to H-bond breaking as the TOS period increases. According to the TGA findings, the carbon yield percentages at 500 °C and 850 °C showed significant increases, reaching 71.4% and 63.5%, respectively, for the sample that underwent heat treatment at 245 °C for 120 min. The incorporation of ferric chloride into the PA6 molecular structure during carbon fiber manufacturing accelerated the stabilization reactions, which could potentially reduce the overall processing costs for final carbon fiber production. This study highlights the appropriateness of using melt-spun PA6 fibers as precursors for carbon fiber manufacturing.

Acknowledgements This research received backing from the YÖK 100/2000 Micro and Nano Technology Materials Ph.D. scholarship, which was awarded by the Higher Education Council of Turkey to Tuba Demirel.

Author Contributions Tuba Demirel: conceptualization, investigation, review and editing, data acquisition, fund acquisition; Kemal Şahin Tunçel: methodology, data analysis, review; Ismail Karacan: writing—original draft, supervision, editing.

Funding Open access funding provided by the Scientific and Technological Research Council of Türkiye (TÜBİTAK). Yükseköğretim Kurulu, YÖK 100/2000, Tuba Demirel.

Data Availability The authors declare that the data supporting the findings of this study are available within the paper. If any raw data files are needed in another format, they are available from the corresponding author upon reasonable request.

Declarations

Conflict of Interest There is no conflict of interest among the authors.

References

1. Md.M. Rahman, T. Demirel, K.Ş Tunçel, I. Karacan, J. Mater. Sci. **56**, 14844 (2021)
2. Y. Ren, T. Huo, Y. Qin, X. Liu, Materials **11**, 483 (2018)
3. D. Jang, M.E. Lee, J. Choi, S.Y. Cho, S. Lee, Carbon **186**, 644 (2022)
4. H. Khayyam, R.N. Jazar, S. Nunna, G. Golkarnarenji, K. Badii, S.M. Fakhrhoseini, S. Kumar, M. Naebe, Prog. Mater. Sci. **107**, 100575 (2020)
5. P. Bhatt, A. Goe, Mater. Sci. Res. India **14**, 52 (2017)
6. E. Frank, F. Hermanutz, M.R. Buchmeiser, Mater. Eng. **297**, 493 (2012)
7. P. Bajaj, D.K. Paliwal, A.K. Gupta, J. Appl. Polym. Sci. **67**, 1647 (1998)
8. X. Guo, L. Liu, H. Feng, D. Li, Z. Xia, R. Yang, Polymers **15**, 2161 (2023)
9. K.-H. Su, J.-H. Lin, C.-C. Lin, J. Mater. Process. Technol. **192–193**, 532 (2007)
10. B.L. Deopura, N.V. Padaki, in *Textiles and Fashion Materials Design and Technology*. ed. by R. Sinclair (Woodhead Publishing, 2015), p.97
11. W.-J. Jin, X.-W. Cheng, W.-L. He, L. Gu, S. Li, Y.-W. Gou, J.-P. Guan, G. Chen, Thermochim. Acta **706**, 179073 (2021)
12. B. Lánská, L. Matisová-Rychlá, J. Rychlý, Polym. Degrad. Stab. **87**, 361 (2005)
13. T. Wang, X. Li, R. Luo, Y. He, S. Maeda, Q. Shen, W. Hu, Thermochim. Acta **690**, 178667 (2020)
14. I. Karacan, K.Ş Tunçel, Polym. Degrad. Stab. **98**, 1869 (2013)
15. I. Karacan, G. Baysal, Fibers Polym. **13**, 864 (2012)
16. I. Karacan, K. Ş. Tunçel, In: Recent Research Development in Applied Polymer Science, ed. By S. G. Pandalai, (Research Signpost, 2013), p. 1.
17. Yu.D. Andrichenko, T.V. Druzhinina, Fibre Chem. **31**, 1 (1999)
18. A.V. Tovmash, A.K. Budyka, V.G. Mamagulashvili, V.A. Rykunov, A.D. Shepelev, B.I. Ogorodnikov, Fibre Chem. **39**, 450 (2007)
19. P. Cerruti, C. Carfagna, Polym. Degrad. Stab. **95**, 2405 (2010)
20. T. Demirel, Md.M. Rahman, K.Ş Tunçel, I. Karacan, Fibers Polym. **23**, 3046 (2022)
21. K.Ş Tunçel, Md.M. Rahman, T. Demirel, I. Karacan, Polym. Eng. Sci. **62**, 1081 (2022)
22. P. Bajaj, A.K. Roopanwal, J. Macromol. Sci. Polym. Rev. **37**, 97 (1997)
23. X. Qin, Y. Lu, H. Xiao, W. Zhao, Polym. Eng. Sci. **53**, 827 (2013)
24. Y. Ge, Z. Fu, Y. Deng, M. Zhang, H. Zhang, J. Mater. Sci. **54**, 12592 (2019)
25. N.S. Murthy, S.M. Aharoni, A.B. Szollosi, J. Polym. Sci. Polym. Phys. **23**, 2549 (1985)
26. F. Auriemma, V. Petraccone, L. Parravicini, P. Corradini, Macromolecules **30**, 7554 (1997)
27. L. Penel-Pierron, C. Depecker, R. Séguéla, J.-M. Lefebvre, J. Polym. Sci. Polym. Phys. **39**, 484 (2001)
28. N. Vasanthan, Text. Res. J. **74**, 545 (2004)
29. I. Abu-Isa, J. Polym. Sci. Polym. Chem. **9**, 199 (1971)
30. H.H. Chuah, R.S. Porter, Polymer **27**, 241 (1986)
31. S.-Y. Kwak, J.H. Kim, S.Y. Kim, H.G. Jeong, I.H. Kwon, J. Polym. Sci. Polym. Phys. **38**, 1285 (2000)
32. S. Murase, M. Kashima, K. Kudo, M. Hirami, Macromol. Chem. Phys. **198**, 561 (1997)
33. Y. Liu, L. Cui, F. Guan, Y. Gao, N.E. Hedin, L. Zhu, H. Fong, Macromolecules **40**, 6283 (2007)
34. T. Demirel, K. Ş. Tunçel, I. Karacan, in Defense Industry Symposium and Exhibition, (Chamber of Mechanical Engineers, Turkey, 2022), p. 234.
35. J.N. Bull, R.G.A.R. Maclagan, C.M. Fitchett, W.C. Tennant, J. Phys. Chem. Solids **71**, 1746 (2010)
36. M. Afshari, A. Gupta, D. Jung, R. Kotek, A.E. Tonelli, N. Vasanthan, Polymer **49**, 1297 (2008)
37. J. Charles, G.R. Ramkumaar, S. Azhagiri, S. Gunasekaran, E. -J. Chem. **6**, 23 (2009)
38. N. Vasanthan, R. Kotek, D.-W. Jung, D. Shin, A.E. Tonelli, D.R. Salem, Polymer **45**, 4077 (2004)
39. D.J. Skrovanek, S.E. Howe, P.C. Painter, M.M. Coleman, Macromolecules **18**, 1676 (1985)
40. T. Demirel, K. Ş. Tunçel, I. Karacan, In International Scientific Research Conference (ASES, Turkey, 2022), p. 73.
41. T. Demirel, Md.M. Rahman, I. Karacan, *International Science and Applied Sciences Congress* (ISPEC, Turkey, 2021), p.277
42. P. Dunn, G.F. Sansom, J. Appl. Polym. Sci. **13**, 1657 (1969)
43. S.J. Cooper, M. Coogan, N. Everall, I. Priestnall, Polymer **42**, 10119 (2001)
44. A. Gupta, C.D. Saquing, M. Afshari, A.E. Tonelli, S.A. Khan, R. Kotek, Macromolecules **42**, 709 (2009)
45. X. Liu, Q. Wu, L.A. Berglund, Z. Qi, Macromol. Mater. Eng. **287**, 515 (2002)
46. A. Siegmann, Z. Baraam, Int. J. Polym. Mater. Polym. Biomater. **8**, 243 (1980)